Strain-mediated elastic coupling in magnetoelectric nickel/barium-titanate heterostructures

Robert Streubel,[1,2,*] Denny Köhler,[1] Rudolf Schäfer,[3,4] and Lukas M. Eng[1]

[1]*Institute of Applied Photophysics, Technische Universität Dresden, 01062 Dresden, Germany*

[2]*Institute for Integrative Nanosciences, Leibniz Institut für Festkörper und Werkstoffforschung Dresden, 01069 Dresden, Germany*

[3]*Institute for Metallic Materials, Leibniz Institut für Festkörper und Werkstoffforschung Dresden, 01069 Dresden, Germany*

[4]*Institute for Materials Science, Technische Universität Dresden, 01062 Dresden, Germany*

(Received 12 December 2012; revised manuscript received 19 January 2013; published 13 February 2013)

Multiferroic nanomaterials bear the potential for assembling a manifold of novel and smart devices. For room temperature (RT) applications, however, only the $BiFeO_3$ single-phase perovskites are potential candidates to date. Nevertheless, vertical heterostructures separating magnetic and ferroelectric functionality into different layers are now widely proposed to circumvent this lack in materials' availability. We show here that the second approach is very profitable as illustrated by the strain-mediated coupling between such two layers, i.e., a ferroelectric barium titanate single-crystal (BTO) and a magnetostrictive nickel (Ni) thin film. Applying an electric field across the BTO substrate forces the magnetic easy axis in the Ni film to rotate by 90°, resulting in a magnetic anisotropy in the range of -1.2 to -33 kJ/m^3. We show that local switching proceeds through the nucleation and growth of straight Néel-domain walls at a cost of zigzag walls. The process is fully reversible and continuously tunable as investigated with magnetooptical Kerr microscopy and magnetic force microscopy probing the local in-plane and out-of-plane magnetizations, respectively. Moreover, the degree of anisotropy can be pre-engineered by depositing the Ni film either at RT, above the Curie temperature T_c of BTO, or at an intermediate temperature. Our findings give evidence for using the reported coupling in modern devices, such as magnetoresistive random access memories, spin valves, spin-polarized electron emission, but equally for the bottom-up assembling of magnetizable molecular nanostructures through magnetic domain wall engineering.

DOI: 10.1103/PhysRevB.87.054410 PACS number(s): 75.30.Gw, 75.60.Ch, 75.80.+q, 75.85.+t

I. INTRODUCTION

For the last decade, much attention has been paid to multiferroic and magnetoelectric (ME) media to understand ferroic ordering phenomena.[1–5] For applications, heterostructures that allow a separate tuning of the physically relevant properties of each layer are particularly promising. In this respect, core-shell heterostructures have been proposed as subwavelength coherent light sources via higher harmonic generation,[6] while ME multilayer structures were shown to be beneficial in low-power spintronic devices[7] and magnetoresistive random access memories.[8]

When varying the lattice constant of the underlying layer/substrate, the magnetic anisotropy of a magnetostrictive top layer can be modified reversibly. This may be initiated through quite different means, i.e., by ion implantation into the substrate,[9] through substrate bending, or by applying an electrical bias voltage across a ferroelectric substrate. To date, however, mostly the integral properties of such ME coupling have been the research focus,[10–13] clearly elucidating the feasibility of such novel devices. In contrast, evaluating and understanding the microscopic coupling and physical mechanisms within such ME heterostructures has not yet been reported. This is necessary to propose adequate material combinations for novel prospective device applications.

Here, we fill this gap and present the possibility of tuning the local strain-induced magnetic anisotropy of a 50-nm-thick magnetostrictive nickel (Ni) film deposited onto a single-crystal barium titanate (sc-BTO) substrate, simply by adjusting the deposition conditions, i.e., the substrate temperature. After Ni deposition, the induced strain is varied by applying an electric field to the BTO substrate, hence varying the substrate lattice constant. As a result, the magnetic domain pattern in the Ni film jumps into a new equilibrium state with partially reoriented magnetic domains. Magnetooptical Kerr microscopy reveals either a parallel or perpendicular alignment of the magnetic easy axis with respect to the ferroelastic domain walls in BTO. In addition, magnetic force microscopy (MFM) inspects both the type of magnetic domain wall, its stability, and dynamics. [Note that Kerr microscopy allows to visualize the in-plane magnetization (xy plane), while MFM probes the magnetic stray field of magnetostatic charges (domain walls) within the Ni film.] Optimized deposition parameters could then be established at an intermediate substrate temperature of 90 °C, allowing the reversible nucleation of magnetic zigzag domain walls[14] upon applying an electric field to the BTO substrate. Moreover, we analyze our findings in the context of an analytical model[15] calculating the strain-induced anisotropy distribution in the Ni film; as shown both the theory and experiment match very well.

II. PREPARATION

A large strain-mediated coupling between the ferroelectric substrate and the magnetostrictive layer is obtained by choosing nickel as the magnetic layer. Its large magnetostriction constant of $\lambda \approx -3.4 \times 10^{-5}$ (Ref. 16) and the low saturation magnetization are superior to minimize the contribution of flux-closure domains over other transition metals, such as Fe or Co. The Ni (50 nm) film was deposited via dc magnetron sputtering onto a ferrolectric (FE) 500-μm-thick sc-BTO substrate with an atomically flat [100] surface. The lattice constants of BTO at room temperature are 3.993 and 4.035 Å along the ferroelectric c (out-of-plane polarization) and a axes (in-plane polarization), respectively,[17] that allow to induce a strain into

the nickel film by applying an electric field after deposition to the substrate. In this way, a maximum in-plane strain-induced anisotropy of $K = (-35 \pm 10)$ kJ/m^3 is feasible. A comparison with the anisotropy of the unstrained nickel film of $K \approx -1$ kJ/m^3 and the crystal anisotropy of $K \approx -4.5$ kJ/m^3 (Ref. 18) clearly demonstrates the benefits and strengths of strain-mediated ME coupling in the Ni/BTO system.

In addition, heating the substrate above its transition temperature of 126 °C transfers the tetragonal symmetry of the unit cell into a cubic one with a lattice constant of 4.01 Å. Since the sputtering ions have a large kinetic energy that is transferred to the target atoms, a small temperature increase of the BTO substrate is present during deposition. In case of a sufficient heat transfer between the nickel atoms and substrate surface, the very surface may exceed the ferroelectric transition temperature. Because the bulk region has a lower temperature, a temperature and strain gradient is generated. By adjusting both the deposition rate and environmental temperature, the lattice constants at the surface are set. In this respect, the samples were prepared at three different deposition conditions (base pressure: 7×10^{-8} mbar; Ar pressure: 10^{-3} mbar): (a) at room temperature using a minimum deposition rate of 3.3 nm/min (NB1); (b) at a high temperature (>126 °C) with a minimum deposition rate of 3.3 nm/min (NB2); and (c) at an intermediate temperature of 90 °C using a maximum deposition rate of 36 nm/min (NB3). No capping layer was used that could modify the stress distribution within the film. In this respect, no precautions to prevent surface oxidation have been made. However, the qualitative behavior is not affected as verified by investigating an one-year-old sample. The nanocrystalline morphology of the resulting films was verified by the lack of both x-ray diffraction reflexes in x-ray diffraction measurements and Kikuchi patterns in electron backscatter diffraction measurements.

III. RESULTS AND DISCUSSION

In our investigations, the BTO substrate temperature was varied in three different runs, explicitly specifying the following three cases for the Ni/BTO (NB) system:

(i) **NB1**: $T_{RT} = 25$ °C: Room temperature deposition of Ni onto sc-BTO, with the BTO showing ferroelectric domains;

(ii) **NB2**: $T > T_c = 126$ °C: Ni is deposited onto paraelectric sc-BTO; and

(iiii) **NB3**: $T_{RT} < T < T_c$: Intermediate state with BTO being ferroelectric during Ni deposition.

Independent of the preparation conditions, all the experiments reported here were carried out at ambient conditions [room temperature (RT), air]. Hence, we observe for all three cases an equilibrium distribution of FE domains in the sc-BTO substrate. Their equilibrium period measures a few micrometers in lateral size[19] and thus allows to use also optical techniques for inspection. BTO at RT splits into ferroelectric a (in-plane) and c (out-of-plane) domains separated by either ferroelastic 90° or ferroelectric 180° domain walls. The effective FE domain distribution as thoroughly checked by piezoresponse force microscopy (data not shown) reveals the antiparallel domain alignment in $a+/a-$ and $c+/c-$ polarization configurations, respectively. Nevertheless, this subtle differentiation does not affect the strain-mediated coupling since only the BTO unit cell form and size within the a- and c-domain areas is of importance. Note that the c- and a-domain unit cells measure 0.3993 × 0.3993 nm and 0.4035 × 0.3993 nm at RT,[17] respectively, with the longer a axes in the second case being aligned perpendicular to the ferroelastic domain wall. Also note that the ferroelastic strain between unit cells that need to match at the 90° domain walls results in a 0.6° surface tilt, often referred to as a topographic step [Fig. 1(a)].

We declare α and β domains that refer to magnetic domains with tensile and compressive stress perpendicular to the topographic steps, respectively. In this respect, the strain-induced magnetic easy axis for negative magnetostrictive nickel is oriented parallel (α) and perpendicular (β) to the topographic steps. In isotropically stressed domains (γ), the magnetization alignment is governed by stray field and exchange minimization.

A. NB1: $T_{RT} = 25$ °C

We first discuss case (i) where the nickel film was deposited at RT (NB1 sample). The low deposition rate of 3.3 nm/min provides a vanishing strain-induced anisotropy due to the stress-free Ni attachment to the BTO surface [Fig. 1(a)]. Magnetic domain patterns were recorded right after Ni deposition by means of MFM. As shown in Fig. 1(b), the as-deposited Ni film splits up into microscopically small magnetic domains with random orientation that are surrounded by cross-tie domain walls (alternating black-white contrast), characteristic for thin films with a very low to moderate magnetic anisotropy.[20,21] The patchy magnetic contrast that refers to a modulation of the magnetization illustrates the nanocrystalline morphology of the film. Moreover, no registry between magnetic and ferroelastic domain walls could be deduced.

Similarly, we analyzed the sample for in-plane magnetization using longitudinal Kerr microscopy; notably, no domains were observed after demagnetizing the sample perpendicular to the sensitive direction. The lack of a contrast in any direction underlines the absence of a strain-induced magnetic easy axis in this Ni film. The isotropic switching field of (2.0 ± 0.5) mT originates from the effective averaging of the nanocrystalline anisotropy due to exchange coupling known as random anisotropy.[22,23] The magnetic anisotropy constant measures $K = \frac{1}{2}\mu_0 M_S H_K = (-1.2 \pm 0.3)$ kJ/m^3 and is listed in Table I together with the measured saturation magnetization M_S and the anisotropy field H_K.

Applying an external electric field (∼2 kV/cm) across the sc-BTO substrate enlarges the c-domain areas [Fig. 1(a)]; microscopically a domains are switched into c domains thus effectively reducing the surface area by ∼1% within switched FE domains (β domains), hence resulting in compressive strain on the nickel film perpendicular to ferroelastic walls. Figure 1(c) depicts the stress domains derived from the topography change in the optical image before and while applying an electric field. Since Ni is negative magnetostrictive, a magnetic easy axis is generated along the compressive stress axis [Fig. 1(a)]. Accordingly, the magnetization aligns perpendicularly to the ferroelastic domain wall, at least in the vicinity of the newly grown c-domain area due to the substantially increased anisotropy [Fig. 1(d)].

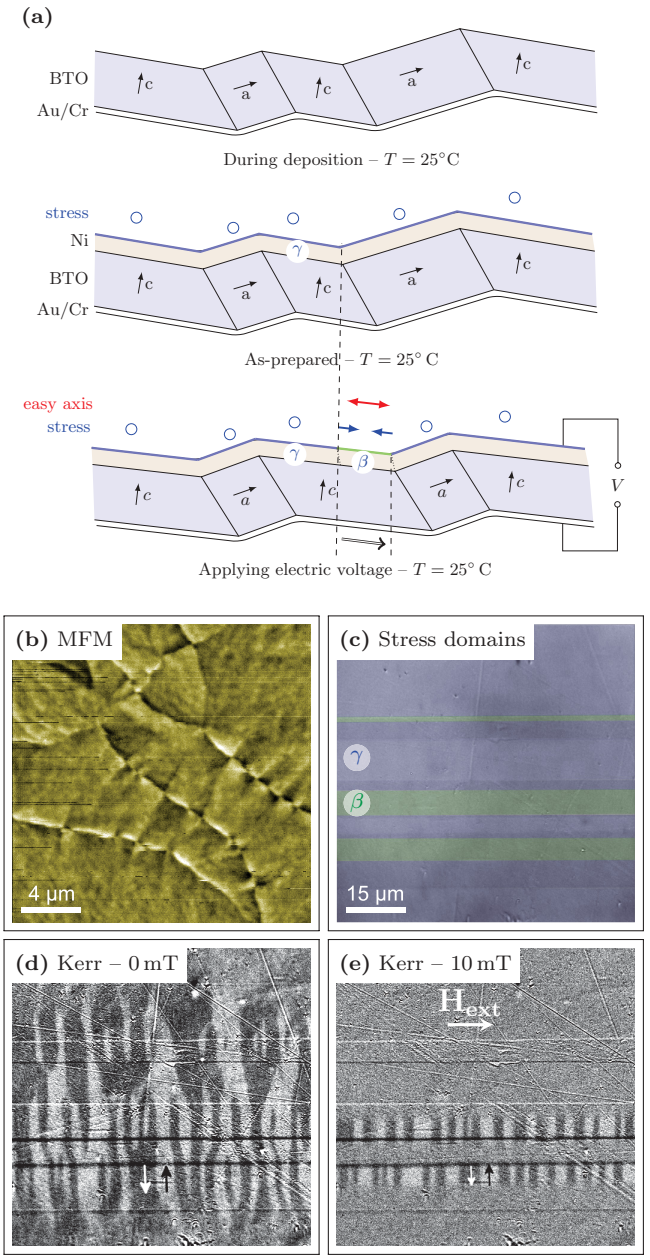

FIG. 1. (Color online) Room temperature deposition of Ni onto BTO (NB1 sample). (a) No effective uniaxial stress is induced into the film (blue regions) when conserving the room temperature lattice constants during deposition. Applying an electric field normal to the surface initiates a ferroelastic phase transition of the substrate that causes uniaxial compressive stress above new c domains (green regions). (b) MFM image of the as-deposited sample shows cross-tie walls randomly distributed throughout the film, indicating low anisotropy. (c) The stress domain distribution of the nickel film exposed to an electric field is depicted. The magnetization component perpendicular to the topographic steps of the demagnetized state is shown in (d). (e) The magnetization of low-anisotropy regions reorients along the direction of the external magnetic field.

Small magnetic domains become visible that broaden with increasing distance from the β domains. Their small size originates from their independent nucleation over the surface at larger fields and the goal to minimize the stray field. We checked this behavior by applying an external magnetic field $H_{\text{ext}} = 10$ mT parallel to the ferroelastic wall as depicted in Fig. 1(e). Comparing the induced magnetic anisotropy in the β domains of $K = (-33.8 \pm 7.5)$ kJ/m^3 with the one in γ domains ($K \approx -1$ kJ/m^3), clearly illustrates the significant strain-mediated coupling.

B. NB2: $T > T_c = 126\,^\circ$C

The second case constitutes an extreme situation in which Ni is deposited onto paraelectric sc-BTO, and then cooled down to RT for inspection (NB2 sample). Initially, the Ni film is stress-free, but experiences locally either an induced tensile or compressive stress upon cooling down to RT. Above a domains, the magnetic easy axis aligns parallel to the ferroelastic domain wall (α domain) even in the absence of any external electric field (not shown). In contrast, the uniform compressive stress above c domains does not generate an easy axis.

Comparing the local anisotropy for these two cases (NB1 and NB2) reveals absolute values on the same order of magnitude (Table I) justifying the equivalence of compression and tension. Moreover, this also suggests that the Ni deposition at an intermediate BTO substrate temperature might provide the desired 90° rotation of the magnetic easy axes upon electric field switching.

C. NB3: $T_{RT} < T < T_c$

At an intermediate substrate temperature of 90 °C, the BTO is still ferroelectric during Ni deposition. In the absence of an electric field, both stress and the magnetic domains are similar to the case at high temperatures (NB2 sample). Nevertheless, the magnitudes of stress and magnetic anisotropy differ considerably. Applying an external electric field generates a magnetic easy axis perpendicular to the ferroelastic domain walls [Fig. 2(a)], and an abrupt transition between α and β domains with charged 90° walls is observed [Fig. 2(c)]. Since the electric voltage (70–200 V) is applied to the whole crystal, merely the density of the α and β domains can be adjusted in this way.

Branching-like domain patterns are formed above ferroelectric c domains to match the different magnetic domain width and minimize the stray field. This separation originates from different switching fields due to distinct magnetic anisotropy (Fig. 3). The position where the magnetic domain wall deviates from its straight direction coincides with the edge of the β and γ domains. An analysis of the widths of these magnetic domains reveals a square-root dependence as expected for Kittel's open domain structures with bulk considerations.[24]

The domain walls are visualized by means of MFM revealing an asymmetric (dipolar) phase contrast for straight Néel walls in β domains and a symmetric (monopolar) phase contrast for head-to-head (h2h)/tail-to-tail (t2t) walls in α domains (Fig. 4). Charged 90° domain walls separate high-anisotropy α and β domains. The magnetic structure depicted in Fig. 4(b) is obtained after partial substrate switching, which results in the annihilation and renucleation of a and hence α domains [Fig. 4(c)]. To minimize the stray field, flux-closure

TABLE I. The table summarizes saturation magnetization M_s, in-plane anisotropy K, and coercive field H_c of the investigated Ni/BTO samples prepared at different temperatures T_{dep}. The good agreement of the Kerr and SQUID values illustrates homogeneity throughout the sample. The calculated anisotropy constant is (-35 ± 10) kJ/m^3.

Sample	T_{dep} [°C]	M_s [kA/m]	Stress domain	K^{Kerr} [kJ/m^3]	K^{SQUID} [kJ/m^3]	H_c^{Kerr} [mT]	H_c^{SQUID} [mT]
NB1	≈25	300 ± 42	γ	-0.5 ± 0.5	-1.2 ± 0.3	1.6 ± 0.5	1.4 ± 0.5
			β	-33.8 ± 7.5	-33.0 ± 7.3	5.7 ± 0.2	–
NB2	⩾126	265 ± 37	γ	-1.5 ± 0.3	-1.2 ± 0.3	8.5 ± 1.0	5.0 ± 0.5
			α	-25.2 ± 5.5	-30.5 ± 6.7	14.5 ± 2.0	14.5 ± 2.0
NB3	≈90	280 ± 39	α	-12.6 ± 2.8	-14.0 ± 3.1	2.0 ± 0.5	1.7 ± 0.5
			β	-22.3 ± 5.1	-23.7 ± 6.2	8.0 ± 1.0	8.0 ± 1.0

domains are formed by inducing h2h/t2t domain walls, which connect the adjacent α domains. In this respect, the zigzag walls nucleate with the anchors pinned at the center of charged

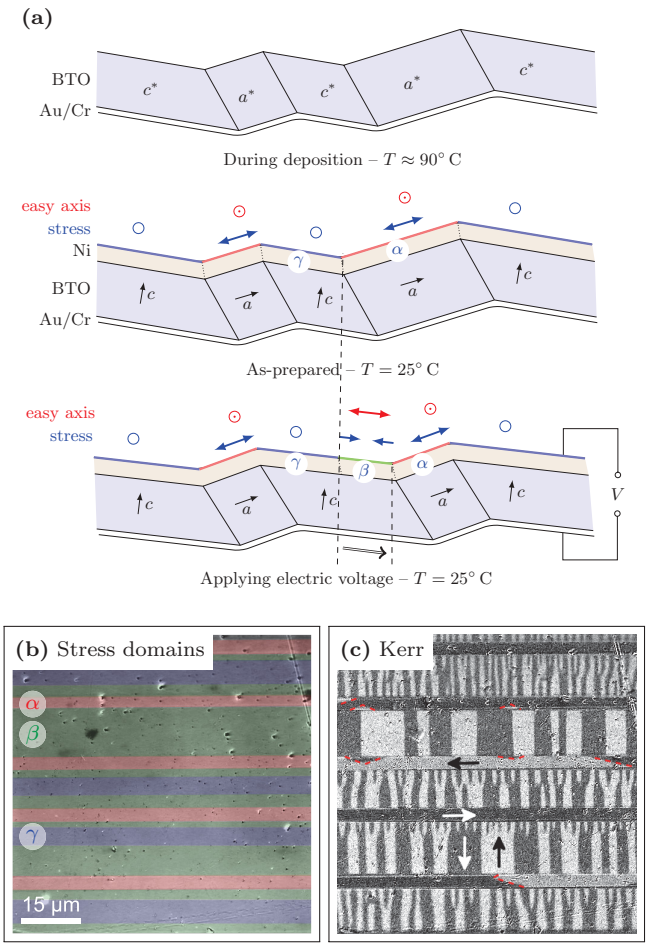

FIG. 2. (Color online) Strain-mediated coupling in magnetoelectric Ni/BTO (NB3 sample). (a) The lattice constants of the substrate during deposition are set by varying both deposition rate and environmental temperature. At room temperature after deposition, uniaxial tensile (α domains, red regions) and isotropic compressive stress (γ domains, blue regions) are induced into the film that generate magnetic easy axes in the nickel film due to magnetostriction. Applying an electric field induces uniaxial compressive stress into the nickel film (β domains, green regions). Images (b) and (c) depict the stress domain distribution and the superimposed in-plane magnetization components of a state demagnetized along the ferroelastic domain walls, respectively.

90° walls of opposite MFM contrast. As a result, periodically alternating h2h and t2t walls with changing magnetic charges appear. As the a-domain area increases, the angle between the wall normal and magnetic easy axis decreases due to the fixed mean orientation of the wall. After exceeding the critical value, the zigzag folding of the magnetic domain wall occurs. In the case of NB3, the zigzag walls align under angles of $(-18.1 \pm 3.9)°$ and $(21.3 \pm 4.5)°$ with respect to the ferroelastic domain wall as shown in Fig. 4(c). The density and position of the zigzag walls are retained while applying an external electric field due to the conservation of the domain width within β domains.

The magnetic hysteresis loops of all three samples were measured by both magnetooptical Kerr microscopy with an information depth of 20 nm and a volume-integrative superconducting quantum interference device (SQUID, VSM, Quantum Design). The saturation magnetizations are derived from the SQUID data that reveals a decrease with increasing temperature (Table I). At a high deposition temperature, the film consists of larger grains with a corresponding lower density due to the enlarged interstitial space. Comparing the absolute values of ≈300 kA/m with that of crystalline Ni (487 kA/m) illustrates a significantly reduced saturation magnetization (0.54–0.62). This distinct value of Ni/BTO was also reported by other groups.[13] Within each deposition run, Ni/BTO and nickel on a Cu plate were simultaneously prepared to access the impact of the substrate. For Ni/Cu, a saturation magnetization of (390 ± 50) kA/m was found. The large spread is assigned to a varying volume density of interstitial spaces and grains due to the substrate lattice constant. Since the BTO substrate is perfectly flat and clean, the interatomic distance can be much more effectively imprinted into the film as in case of a Cu plate.

The extraordinary low magnetization was verified by both electron beam vapor deposition and sputtering, and measured by two different SQUIDs. Another proof could be given by calculating analytically the magnetostrictive anisotropy constant. For this purpose, the so-called coherency technique[15,26] was adapted to describe an amorphous isotropic thin film, whose bottom surface is strained according to the change of the lattice constants of the substrate due to either thermal or electric phase transition. Within this framework, the back coupling of the film, elastic, and further magnetic energy contributions are neglected. Both the tilt and lattice change are described by infinitesimal edge dislocations with Burgers vectors normal and parallel to the surface, respectively. For further insight,

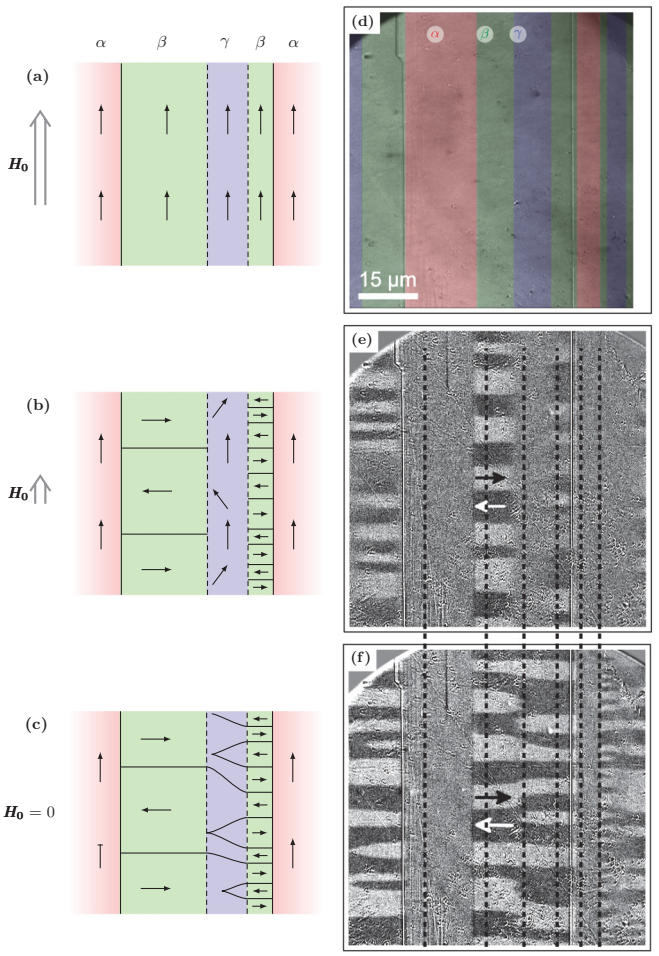

FIG. 3. (Color online) Branching-like domain patterns in $\beta/\gamma/\beta$ sandwich structures. The three panels (a)–(c) illustrate the switching behavior of β domains in the vicinity of γ domains in a longitudinal magnetic field, shown at the right [(d) stress domains; magnetic domains via MOKE imaging (e)–(f)]. (a) Sufficiently large fields cause a saturation along their direction. (b, e) Below the switching field of β domains (≈20 mT), the magnetization rotates into the easy axis. The magnetization within the embedded γ domains is still aligned along the field direction due to much smaller anisotropy. Because the system tends to reduce the net charge of domain walls, the vectors within γ domains slightly tilt with decreasing field. (c, f) The resulting remanence state exhibits branching-like domain patterns with a tilt of magnetization to match the different domain widths within the neighboring β domains. The mean tilt and mean width can be adjusted by applying different magnitude of normal electric field to change the underlying ferroelectric domain structure. In this respect, the bottom-up assembling of magnetizable molecules can be controlled.

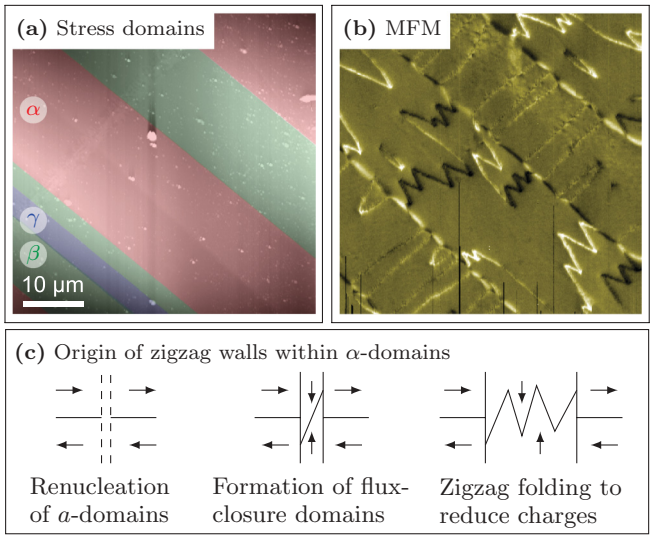

FIG. 4. (Color online) Domain wall configuration in magnetoelectric Ni/BTO. Panels (a) and (b) show stress domains and corresponding domain wall configuration with zigzag walls and straight Néel walls located above a and c domains, respectively. The origin of zigzag walls is sketched in (c). Decreasing the electric voltage after saturation, new a and α domains nucleate. To reduce the stray field, flux-closure domains are formed exhibiting head-to-head/tail-to-tail configurations. The angle of the domain wall increases further with decreasing voltage due to pinned anchor points that eventually induce a zigzag folding.

we refer to the original work.[15,26] For calculations, the shear modulus $\mu = \kappa_{\text{nano}} \cdot 40.5$ GPa and the Poisson ratio $\nu = 0.3$ of polycrystalline nickel[25] are used. The coefficient $\kappa_{\text{nano}} = 0.54 \pm 0.23$ accounts for the low nickel density, assuming a linear relation between elastic coefficients and volume density. The values $[(-35 \pm 10)\ \text{kJ/m}^3]$, obtained for the coercive field and anisotropy shown in Table I, agree well with our Kerr and SQUID measurements, which demonstrates homogeneity throughout the sample and properly derived shear modulus/volume density. The success of adapting the theory provides a way to predict both stress and its continuous transition from compressive to tensile as it is important for miniaturization/application.

IV. SUMMARY

In conclusion, we demonstrated the possibility of influencing the strain-induced anisotropy in ME Ni/BTO heterostructures by using appropriate preparation conditions and adequate external electric fields. In this respect, the tensile and compressive stresses of a different magnitude are induced into the magnetostrictive Ni film after deposition, generating a magnetic easy axis that is aligned either parallel or perpendicular to the ferroelastic domain walls. Appropriate deposition parameters allowed a local rotation of the magnetic easy axis by 90° driven by an external electric field, which makes this approach attractive for spintronics devices and spin valve sensors since they need the adjustable sensitivity for in-flow detection of magnetic particles.[27] In contrast to Ref. 28, where zigzag walls were nucleated randomly by applying a local magnetic field, the predefined straight Néel walls in β domains determine the anchor points (center of 90° wall depends on the separation between straight Néel walls) and a real density of the magnetic zigzag walls whose nucleation is electrically driven. The corresponding reversible nucleation of zigzag domain walls driven by electric fields as well as the different stability of magnetic zigzag and straight Néel walls above ferroelectric a and c domains, respectively, allows to sense magnetic microparticles and probably even

nanoparticles at the microscale by measuring the change of magnetoresistance due to the deformation/annihilation of domain walls.[29–31] The reversibility and electric field-driven motion of magnetic domain walls makes the investigated system also very attractive for the bottom-up assembling of magnetic beads or molecular nanostructures and microstructures and their controlled manipulation.[32–34]

ACKNOWLEDGMENTS

The authors thank A. Wolter and C. Krien (IFW Dresden) for providing the opportunity to measure SQUID VSM and metal deposition, respectively, and C. Patschureck for support with Kerr microscopy. N. Farag and M. Bobeth (TU Dresden) are acknowledged for fruitful discussions. D.K. thanks the DFG under Project No. RTG-1401 for financial support.

*r.streubel@ifw-dresden.de

[1] H. Schmid, Ferroelectrics **162**, 317 (1994).
[2] T. Kimura, T. Goto, H. Shintani, K. Ishizaka, T. Arima, and Y. Tokura, Nature (London) **426**, 55 (2003).
[3] N. A. Spaldin and M. Fiebig, Science **309**, 391 (2005).
[4] W. Eerenstein, N. D. Mathur, and J. F. Scott, Nature (London) **442**, 759 (2006).
[5] R. Ramesh and N. A. Spaldin, Nat. Mater. **6**, 21 (2007).
[6] Y. Pu, R. Grange, C.-L. Hsieh, and D. Psaltis, Phys. Rev. Lett. **104**, 207402 (2010).
[7] V. Garcia, M. Bibes, L. Bocher, S. Valencia, F. Kronast, A. Crassous, X. Moya, S. Enouz-Vedrenne, A. Gloter, D. Imhoff, C. Deranlot, N. D. Mathur, S. Fusil, K. Bouzehouane, and A. Barthélémy, Science **327**, 1106 (2010).
[8] J.-M. Hu, Z. Li, L.-Q. Chen, and C.-W. Nan, Nat. Commun. **2**, 553 (2011).
[9] J. McCord, I. Mönch, J. Fassbender, A. Gerber, and E. Quandt, J. Appl. Phys. D **42**, 055006 (2009).
[10] C.-W. Nan, Phys. Rev. B **50**, 6082 (1994).
[11] W. Eerenstein, M. Wiora, J. L. Prieto, J. F. Scott, and N. D. Mathur, Nat. Mater. **6**, 348 (2007).
[12] C. Thiele, K. Dörr, O. Bilani, J. Rödel, and L. Schultz, Phys. Rev. B **75**, 054408 (2007).
[13] S. Geprägs, A. Brandlmaier, M. Opel, R. Gross, and S. T. B. Goennenwein, Appl. Phys. Lett. **96**, 142509 (2010).
[14] L. A. Finzi and J. A. Hartmann, IEEE Trans. Magn. **4**, 662 (1968).
[15] A. E. Romanov, W. Pompe, and J. S. Speck, J. Appl. Phys. **79**, 4037 (1996).
[16] E. W. Lee, Rep. Prog. Phys. **18**, 184 (1955).
[17] W. D. Kingery, H. K. Bowen, and D. R. Uhlmann, *Introduction to Ceramics*, 2nd ed. (Wiley, New York, 1976).
[18] J. C. Anderson, Proc. Phys. Soc. **78**, 25 (1961).
[19] M. Holt, K. Hassani, and M. Sutton, Phys. Rev. Lett. **95**, 085504 (2005).
[20] E. E. Huber, Jr., D. O. Smith, and J. B. Goodenough, J. Appl. Phys. **29**, 294 (1958).
[21] A. Hubert and R. Schäfer, *Magnetic Domains*, 3rd ed. (Springer, New York, 2009).
[22] M. Fähnle, C. Elsässer, J. Furthmüller, R. Pawellek, E. H. Brandt, and M. C. Böhm, Physica B: Condensed Matter **161**, 225 (1989).
[23] R. Schäfer, in *Nanoscale Magnetic Materials and Applications*, edited by J. P. Liu, E. Fullerton, O. Gutfleisch, and D. Sellmyer (Springer, New York, 2009), pp. 275–307.
[24] C. Kittel, Phys. Rev. **70**, 965 (1994).
[25] D. C. Hurley, R. H. Geiss, M. Kopycinska-Müller, J. Müller, D. T. Read, J. E. Wright, N. M. Jennett, and A. S. Maxwell, J. Mater. Res. **20**, 1186 (2005).
[26] N. Farag, M. Bobeth, W. Pompe, and A. E. Romanov, Philos. Mag. **87**, 1478 (2007).
[27] I. Mönch, D. Makarov, R. Koseva, L. Baraban, D. Karnaushenko, C. Kaiser, K.-F. Arndt, and O. G. Schmidt, ACS Nano **5**, 7436 (2011).
[28] M. Labrune, S. Hamzaoui, C. Battarel, I. Puchalska, and A. Hubert, J. Magn. Magn. Mater. **44**, 195 (1984).
[29] G. Tatara and H. Fukuyama, Phys. Rev. Lett. **78**, 3773 (1997).
[30] P. M. Levy and S. Zhang, Phys. Rev. Lett. **79**, 5110 (1997).
[31] T. Taniyama, I. Nakatani, T. Namikawa, and Y. Yamazaki, Phys. Rev. Lett. **82**, 2780 (1999).
[32] G. Vieira, T. Henighan, A. Chen, A. J. Hauser, F. Y. Yang, J. J. Chalmers, and R. Sooryakumar, Phys. Rev. Lett. **103**, 128101 (2009).
[33] G. Ruan, G. Vieira, T. Henighan, A. Chen, D. Thakur, R. Sooryakumar, and J. O. Winter, Nano Lett. **10**, 2220 (2010).
[34] E. Rapoport and G. S. D. Beach, Appl. Phys. Lett. **100**, 082401 (2012).